Egyptian Journal of Chemistry

http://ejchem.journals.ekb.eg/

Aluminum 6061 Alloy Modification with Micro Arc Oxidation and Ferric Oxide Nanoparticles Incorporated to Reduce Aluminum Corrosion

Mohannd Kadhim Alshujerya [1] , Khulood Abid Saleh Al-Saadiea [2]

[1] *Department of Chem., College of science, Baghdad University, Baghdad, Iraq, Iraq*

[2] *Department of Chem., College of science, Baghdad University, Baghdad, Iraq*

Abstract:

The MAO approach was used to create incorporation coatings containing Fe_3O_4 nanoparticles on an Aluminium 6061 (A6061) alloy. The effect of nanoparticles on the microstructure and corrosion resistance of produced ceramic composite coatings, as well as the method of their assimilation into the MAO layer, were investigated. Fe_3O_4 nanoparticles were added to an electrolyte solution of its components (10 g/L KH_2PO_4 + 2g/L NaOH), and a high variable AC voltage of 150 volts is applied, to produce MAO composite coatings, a titanium sheet was employed as a counter electrode. Electrochemical impedance spectroscopy (EIS) and polarization experiments were also used to investigate corrosion protection, revealing a strong corrosion protection effectiveness even at temperatures ranging from 298k to 328 K in a saline medium. Where the corrosion current density increase with the increase in temperature. The activation energy and the pre-exponential factor (kinetic parameters) were computed and explained. Furthermore, the thermodynamic values ΔG* and ΔH* were estimated. The impact of nanoparticles on phase composition was investigated using X-ray diffraction (XRD) techniques. Furthermore, scanning electron microscopy (SEM) images indicated the ability of Fe_3O_4 nanoparticles to fill the inherent pores of MAO coatings.

Keywords: Aluminum alloy; Micro arc oxidation; incorporation; nanoparticles; surface treatments

1. Introduction:

Aluminum alloy 6061 (A6061) is an aluminum alloy containing magnesium and silicon as primary alloying components. Because of the alloying elements employed, A6061 provides improved corrosion resistance, formability, weldability, and anodizing response(1-3). It is widely employed in a variety of applications, including home structures, cell phone cases, and automobiles(3-5). Even though A6061 has good corrosion resistance, corrosion can occur attributable to intermetallic particles in the alloy. As a result, various surface treatments are frequently used to protect the alloy against corrosion(6). One of them is Micro arc oxidation (MAO) is a highly recommended procedure for producing a protective oxide film on light metal alloys such as aluminum, zirconium, titanium, and magnesium. The MAO is currently commonly utilized as a helpful coating process to generate oxide layers on the metal; it is a high-voltage mix of electrochemical oxidation, thermal diffusion, and plasma interactions. The massive micro-arc discharges that occur throughout the MAO method significantly raise the local temperature and pressure, resulting in the oxide layer repeatedly melting and solidifying(7).The MAO method is somewhat like anodizing, porous has two layers: an inner barrier layer and an outer porous layer. Because of its compact dense structure, the inner barrier layer is essential for corrosion resistance(8, 9). The outer porous layer is made up of hexagonal cells with a single cylindrical pore in the center of each cell, which contributes to its absorption properties(10). As a result, the electrolyte composition and temperature, working substrate type, working voltage, applied current density, and oxidation duration are all factors that impact the quality of the formed layer on the substrate. The electrolyte composition, in particular, is the most effective element in producing the necessary coating(11).

Several properties, such as good interface adhesion, good surface attractiveness, and improved

Receive Date: 19 July 2022, Revise Date: 01 August 2022, Accept Date: 29 August 2022.
DOI: 10.21608/EJCHEM.2022.151127.6542

mechanical and anti-corrosive capabilities, maybe improved after MAO(12). In general, the MAO process is divided into three stages. The first phase is surface preparation, which is utilized to regulate the quality of the surface. The second stage is MAO, which produces an anodic oxide coating, and the last stage is sealing, which closes oxide pores. To obtain an anodized aluminum surface, major procedures have been patented(13). It has been observed that adding various types of nanoparticles to electrolytes results in a composite coating with desirable qualities. The nanoparticles were dispersed equally throughout the coating, filling the microspores and decreasing the roughness and porosity of the coatings consequently Aluminum-based alloys Fe_3O_4 NPs have been used to improve the properties and characteristics of coatings. The precise control of the size of nanoparticles in the suspension is needed and aggregation of nanoparticles must be avoided. In this work, we have proposed a new method to modify the surface of A6061 by using the electrochemical method of MAO and incorporating nanoparticles simultaneously into the porous layer of Micro arc oxidized Aluminum 6061 (MA6061). This process is carried out during the MAO process.

2. Experimental part

Before MAO, Aluminum specimens have a diameter of 2.5 cm2 and a thickness of 0.5 mm were produced by press cutting of commercially high purity A6061 sheet. The samples were polished with a different emery paper with grit 600, 800, 1000, 1200, and 2000, and then it was polished to a semi-mirror. After polishing the samples were washed with distilled water, and then placed in an ultrasonic bath with acetone for five minutes, then rinsed with distilled water, dried, and finally kept in the desiccator. Then the aluminum samples were treated by immersing them in 10% NaOH for 30 seconds to oxidize the surface,

Followed by a rinse with distilled water to remove the sodium hydroxide remnants and the oxidized layer was removed by immersing in 50% HNO3 until the black oxide layer was removed. Finally, to remove the acid residue and prepare the samples for Micro arc oxidation, they were washed with distilled water.

The anode of the MAO cell is an aluminum alloy, and the cathode is a big piece of steel. These electrodes are immersed in an electrolyte solution of its components (10g/L KH2PO4 + 2g/L NaOH), and a high variable AC voltage of 150 volts is applied. with an inter-electrode spacing of up to 4 cm, To keep the electrolyte temperature as stable as possible, the cell was immersed in an ice bath. To incorporate Fe_3O_4 nanoparticles in Aluminum oxide nanopore that formed during the MAO process, 0.1wt% nanoparticles were added to the electrolyte solution.

After 180 seconds, process with and without nanoparticles finishing, samples were removed, rinsed with cold distilled water then immersed in boiled water for two minutes (to seal the nanopores), dried, and placed in containers to be tested later. The morphologies of the treated aluminum were observed by field emission scanning electron microscopy (FE-SEM) and the chemical composition of samples were measured by X-ray diffraction (XRD).

A WENKING M Lab. (Germany) equipment was used to measure the polarization. Polarization curves for A6061 were obtained before and after MAO. The working, counter, and reference electrodes were A6061, Pt, and Ag/AgCl (sat. KCl (aq)), respectively. As a corrosive medium, saline (3.5% NaCl) solutions were applied.

3. Results and Discussion:

3.1. Chemical structure and morphology of oxide layer :

The FESEM and XRD techniques showed the morphology and chemical structures of the oxide layer formed on A6061 with and without incorporated ferric oxide in the nanopore, respectively (Figure 1 and Figure 2). During the anodizing processes of all samples (MA6061, and MA6061+Fe_3O_4) a high variable AC voltage of 150 volts is applied. In the absence of nanoparticles, a layer of aluminum oxide with non-uniform micropores was formed on the surface of the anodized sample (MA6061), where the diameter of formed pores was 215 nm as shown in (Figures 1). It was observed that adding 4 nanoparticles to the electrolytes of the MA6061+Fe_3O_4 samples (Figure 2) has filled the porous with nanoparticle oxide and the pore size becomes 159.5 nm with Fe_3O_4 incorporation. Nanoparticles were distributed throughout the surfaces of these oxide layers, filling the majority of the microspores. Furthermore, as can be shown, the majority of these integrated nanoparticles are not recognizable and are detected with a size bigger than their main diameter. Indeed, the electrophoretic force attracts nanoparticles to the surface of the sample (anode) and causes them to cover the surface and fill the microspores of the coatings.

The X-ray diffraction features of the Anodized aluminum oxide and the incorporated Fe_3O_4 formed on A6061 by the micro-arc oxidation method are shown in Figure 3. The phases may be seen in all of the XRD patterns. Furthermore, due to the thinness of the oxide layer, the matching peaks to the aluminum substrate were identified in all XRD spectrums. However, peaks of Al_2O_3 (the oxide of the A6061 substrate) were found in these patterns.

The average particle size of incorporated nanoparticles induced using the current electrochemical process may be calculated using Debye–approximation Scherrer's from the peaks' full width at half maximum (FWHM). (Eq. 1)(14).

$$\mathbf{d= k\lambda/\beta\cos\theta \quad \dots (1)}$$

Where d is the crystallite size, k is the CuKa radiation wavelength (k = 1.542A°), β is the FWHM for the diffraction peak in concern (in radians), θ is the diffraction angle, and k is Scherer constant and its value is 0.89). The small peaks at 2θ (38°, 42°, and 65°) referred to γ-Al2O3. The crystallite size has been detected for Al_2O_3 formed on AA6061 without nanoparticles and has an average size equal to (19.8 nm) (Figure 3).

The incorporation of nanoparticles slightly affects the peak positions are slightly shifted to higher 2-theta (2θ) values compared to that AA6061 without nanoparticles.

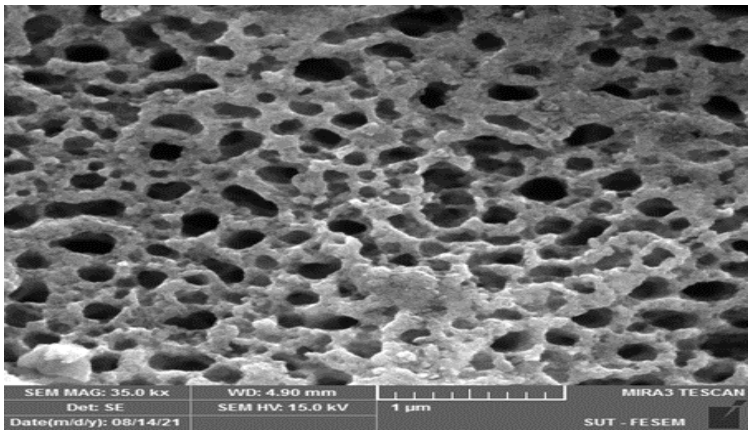

Figure 1. FESEM image of MA6061 with 35000-x magnification

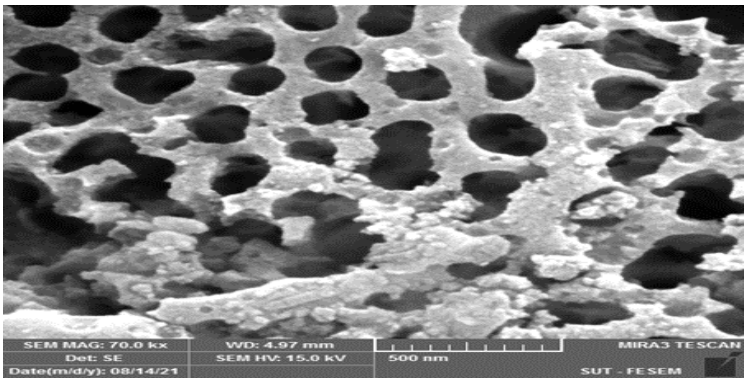

Figure 2. FESEM image of MA6061+ Fe3O4 Nps with 35000-x magnification

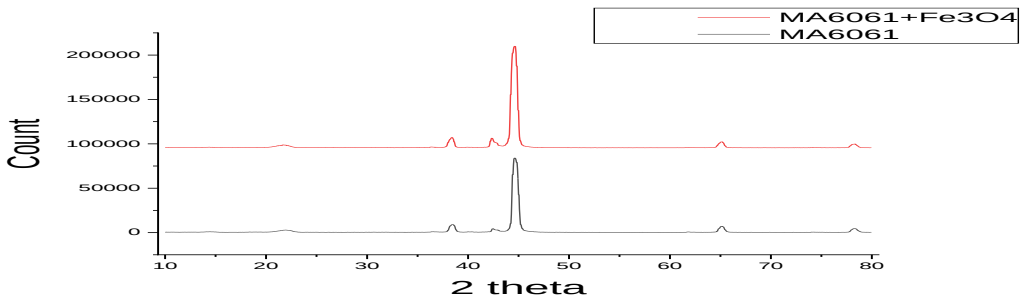

Figure 3. The XRD spectra of the anodized sample

3.2. Corrosion test:

Figure (4) represents the Tafel curves for the corrosion test on A6061 with Micro arc Oxidation and oxide nanoparticles incorporated at various temperatures. The corrosion potential of blank A6061 is shown by the polarization curves (-718.7 to -748.7 mV). After MAO the potential shifted to (-632 mV) at 298K, and the E_{Corr} further shifted to, 494.1 mV compared with figure 4.c. after A6061 was incorporated with Fe_3O_4 NPs

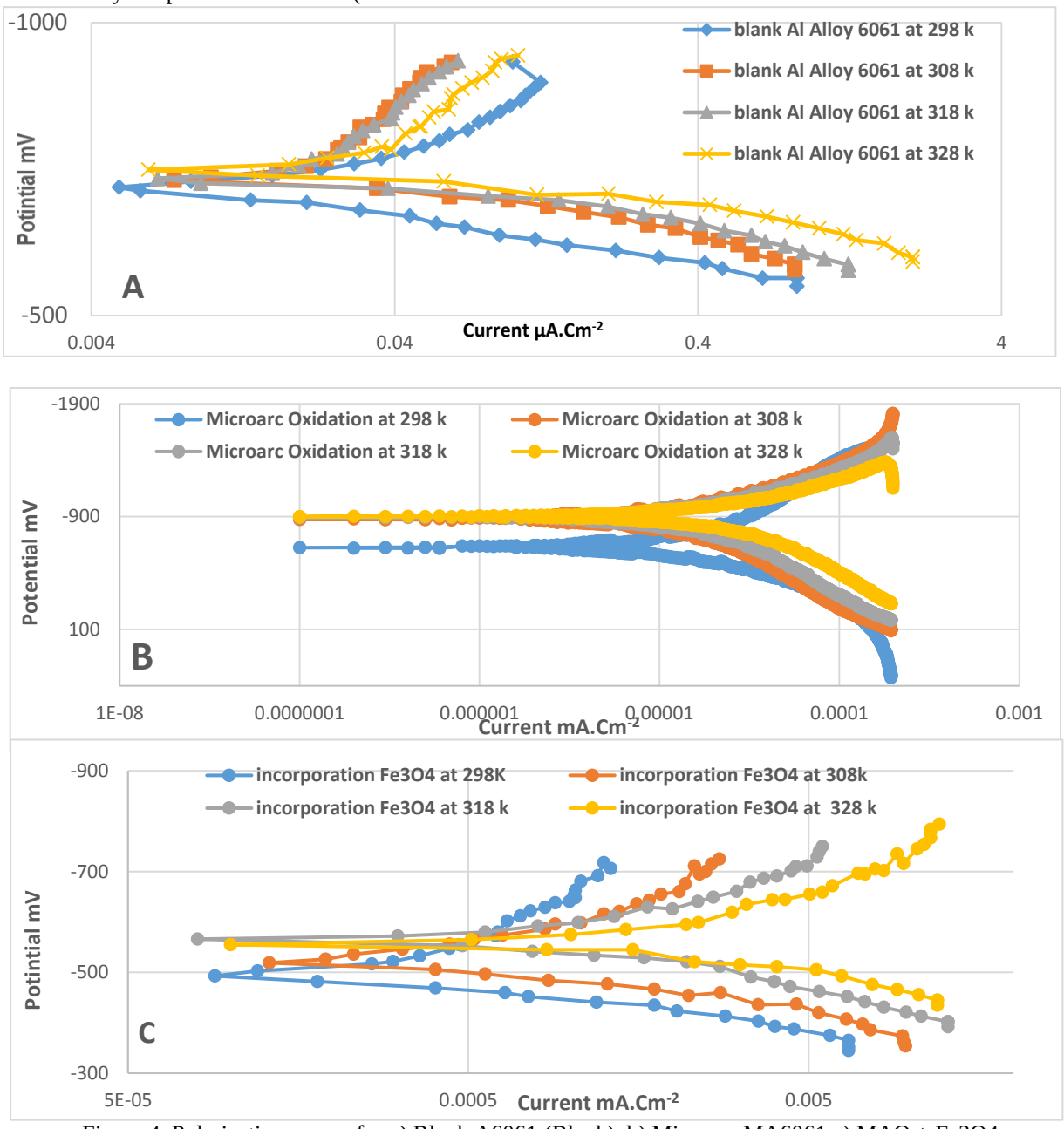

Figure.4. Polarization curves for a) Blank A6061 (Blank), b) Microarc MA6061 c) MAO + Fe3O4

The corrosion current density has significantly raised as the temperature increased for Blank A6061, but after Micro arc oxidation, the corrosion current density decreased from 15.73 microamperes to 0.486 microamperes, and the I_{Corr} value further reduced to the Nanoampere value with the Fe_3O_4 Nanoparticle incorporated. These results indicate that Microarc oxidation and incorporation improve the corrosion resistance of A6061.The Protection Efficiency (% PE) mightbe computed using the equation below(15).

$$\%PE = ((I_{Corr})b - (I=)t)/(I=)b \times 100 \ldots\ldots\ldots (2)$$

Where (I_{Corr}) b and (I_{Corr}) t are the corrosion current density (µA.cm-2) for A6061 (Blank) and treated AA6061after anodizing respectively.

Table.1. Corrosion kinetic parameters for Protective Aluminum 6061 alloy in seawater at the temperatures range (298-328) K.

Temp./K		E_{Corr}/mV	I_{Corr}/µA.cm^{-2}	bc/mV.dec^{-1}	ba/mV.dec^{-1}	w.l/g.m^{-2}.dl^{-1}	P.L/mm.y^{-1}	R_p / Ω.cm	PE%
Uncoated	298	-718.7	15.73	141.3	109.1	1.27	0.171	1699	-
	308	-730.3	20.55	476.3	57.3	1.65	0.224	1081	-
	318	-738.8	26.3	477.8	61.8	1.79	0.243	903	-
	328	-748.7	31.83	495.6	75.8	2.56	0.346	897	-
After MAO	298	-632	0.486	350.7	423.3	0.00044	0.00006	1713	96.9103
	308	-778.9	0.693	747.9	689.4	0.00061	8.24E-05	2247	96.6277
	318	-761.7	0.837	528.1	460.5	0.000674	9.11E-05	1276	96.8174
	328	-899.8	1.2	68.5	54.5	0.000823	0.000111	1098	96.2299
MAO with Fe_3O_4	298	-494.1	0.262	243	80	0.021	0.00285	9974	98.3343
	308	-531.5	0.387	163.3	96.1	0.0312	0.00421	6787	98.1167
	318	-565.4	0.616	132.3	105.3	0.0496	0.0067	4133	97.6577
	328	-555	0.93	170.7	92.6	0.0989	0.00014	2803	97.0782

The best % PE was observed after MA6061 Micro arc Oxidation, which gave a % PE of 96.9% at 298K; nevertheless, table (1) data reveals that %PE don't change as temperature increased, illustrating that I_{Corr} for MA6061 was don't affected by temperature. While the best % PE was obtained after MA6061 was incorporated with Fe_3O_4, which gave a % PE of 98.33% at 298K, The best PE % was acquired with Fe_3O_4 incorporation at 98.33% at 298K, the PE% for incorporated MA6061 slightly decreased with temperature increasing, indicating that I_{Corr} for incorporated AA6061 was not affected by temperature change.

Near the corrosion potential E_{Corr}, there is a little amount of polarization. Therefore, the following equation, known as the Stern–Geary equation (16), is used to determine corrosion resistance:

$Rp = \Delta E/\Delta i = (ba * bc)/(2.303*(ba + bc))*1000$ … (3)

Rp denotes the polarization resistance of the system, ΔE denotes the difference between the polarization potential E and the corrosion potential E_{Corr}, ΔI denotes the difference between the observed current density I and the corrosion current density I_{Corr}, and b_a and b_c denote the anodic and cathodic Tafel coefficients, respectively.

The measurement of entire polarization curves is required when discussing polarization resistance and it is especially useful in diagnosing corrosion problems and initiating reconditioning action(17).

3.3. Kinetic Parameters and the Thermodynamic Studies

The Arrhenius equation might be used to calculate the change in entropy (ΔS*) for the transition, state of corrosion process:

Log I_{Corr}/T=log R/Nh +ΔS^*/2.303R - ΔH^*/2.303RT….. (4)

Where I_{Corr} is the A6061 corrosion current density calculated from the Tafel plot, h is the Plank's constant, N is the Avogadro number, ΔS* is the activation entropy, and ΔH* is the activation enthalpy. The slope of (-ΔH* / 2.303 R) and the intercept of [(log (R/Nh) + (ΔS*/2.303 R)] were derived from the plot of log I_{Corr}/T versus 1/T, from which the values of ΔH* and ΔS*, respectively, were estimated. The data in table (2) shows that after treating the surface of MA6061, the values of entropy changed slightly. Figure (5) shows the plot of log I_{Corr}/T against 1/T.

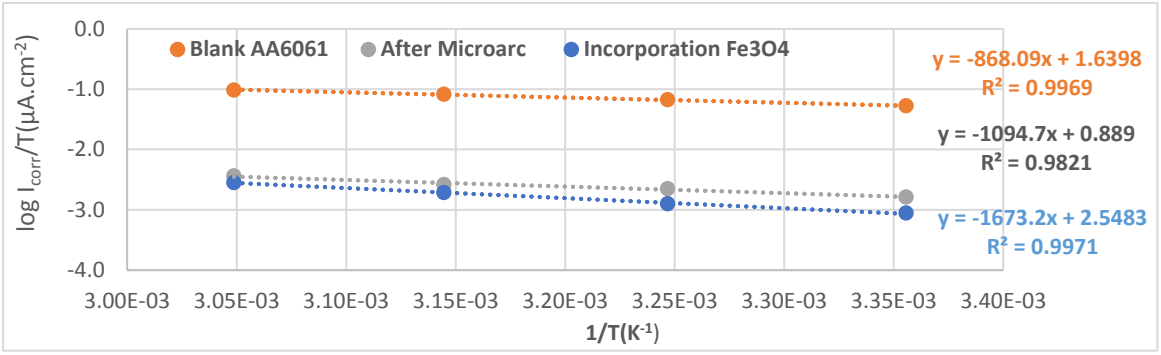

Figure.5. Kinetic and thermodynamic parameters for the corrosion Protective of Aluminium 6061 alloy in seawater at the temperatures range (298-328) K.

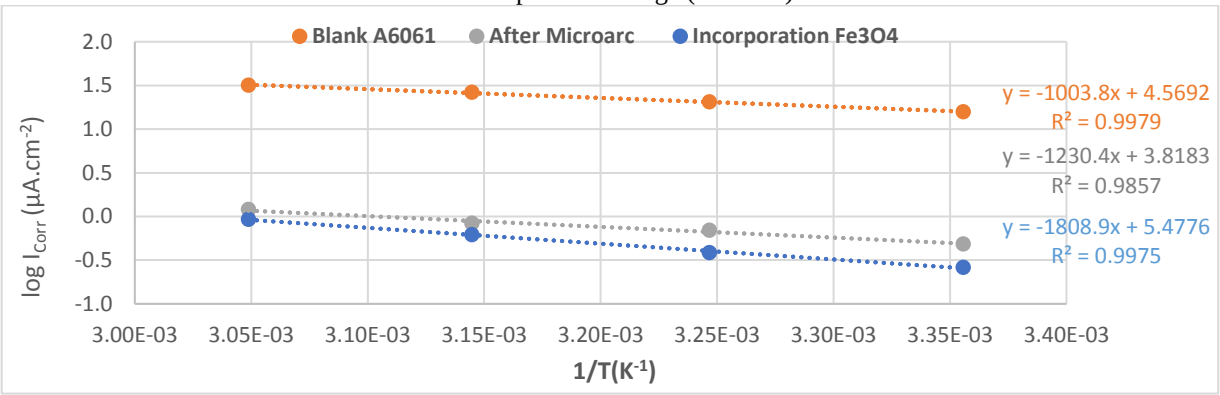

Figure.6. Arrhenius Plot of log I_{Corr}. Versus 1/T for the corrosion for Protective Aluminium 6061 alloy in seawater at the temperatures range (298-328) K

Table.2. Kinetic and thermodynamic parameters for the corrosion Protective of Aluminium 6061 alloy in seawater at the temperatures range (298-328) K.

Temp.(K)		1/T(K^{-1})	E_{Corr}/ mV	I_{Corr} /µA.cm^{-2}	Log I_{Corr}	-ΔG/ kJ.mol^{-1}	ΔH/ kJ.mol^{-1}	ΔS/ J. K^{-1}.mol^{-1}	Ea/ kJ. mol^{-1}	A Molecules.c m^{-2} .S^{-1}
Uncoated	298	0.0034	-718.7	15.73	1.20	66.14	16.62	-0.17	19.2	2.23E+28
	308	0.0032	-730.3	20.55	1.31	67.80				
	318	0.0031	-738.8	26.30	1.42	69.46				
	328	0.0030	-748.7	31.83	1.50	71.12				
After MAO	298	0.0034	-632.0	0.49	-0.31	74.76	20.96	-0.18	23.6	3.97E+27
	308	0.0032	-778.9	0.69	-0.16	76.57				
	318	0.0031	-761.7	0.84	-0.08	78.37				
	328	0.0030	-899.8	1.20	0.08	80.18				
MAO with Fe_3O_4	298	0.0034	-494.1	0.26	-0.58	76.37	32.04	-0.15	34.6	1.81E+29
	308	0.0032	-531.5	0.39	-0.41	77.86				
	318	0.0031	-565.4	0.62	-0.21	79.35				
	328	0.0030	-555.0	0.93	-0.03	80.83				

4. Conclusion

The electro-modification of the A6061 surface with Microarc Oxidation and nanoparticle incorporation provided a better barrier film on aluminum. Microarc oxidation of aluminum reduces the corrosion potential at low temperature also reduces the current density, the protection efficiency was 96 % at all

temperature, and it stay approximately stable raised as the temperature raised. While the best %PE was obtained after MA6061 was incorporated with Fe_3O_4, which gave 98.33 % at 298K The apparent activation energy of MA6061 is23.559kJ/mol while these increases in activation energy result increase in the activation sites and indicated by the Arrhenius factor and this increase in Arrhenius factor due to decrease in corrosion rate.

The free energy change ΔG* values for MA6061 handled with Microarc oxidation and incorporation increased from (66.138 kJ.mol-1) to (74.761kJ.mol-1), and (76.370kJ.mol-1) with Microarc, and "Microarc oxidation + Fe_3O_4 incorporation" respectively at 298K. MA6061 and MA6061+ Fe_3O_4 incorporation resulted in a higher change in enthalpy, activation energy (Ea), and corrosion site number (A) indicating that corrosion requires more energy in this case. These results are in excellent agreement with the protection efficiency results. The average partials size of the diameter of formed pores was 215 nm, while the average, from XRD data, was (19.8 nm).These results qualify our work to be applied in surface modification.

5. References:

1. Khojastehnezhad VM, Pourasl HH. Microstructural characterization and mechanical properties of aluminum 6061-T6 plates welded with copper insert plate (Al/Cu/Al) using friction stir welding. Transactions of Nonferrous Metals Society of China. 2018;28(3):415-26.
2. Salloomi KN. Fully coupled thermomechanical simulation of friction stir welding of aluminum 6061-T6 alloy T-joint. Journal of Manufacturing Processes. 2019;45:746-54.
3. Cavallo C. All About 6061 Aluminum (Properties, Strength and Uses). thomasnet,[Online] Available: https://www thomasnet com/articles/metals-metal-products/6061-aluminum/[Accessed March 2021]. 2021.
4. Venukumar S, Baby B, Muthukumaran S, Kailas SV. Microstructural and mechanical properties of walking friction stir spot welded AA 6061-T6 sheets. Procedia materials science. 2014;6:656-65.
5. Dorbane A, Ayoub G, Mansoor B, Hamade R, Kridli G, Imad A, editors. Mechanical Response and Evolution of Damage of Al6061-T6 Under Different Strain Rates and Temperatures. Proceedings of the TMS Middle East—Mediterranean Materials Congress on Energy and Infrastructure Systems (MEMA 2015); 2015: Springer.
6. Almashhadani HA, Alshujery MK, Khalil M, Kadhem MM, Khadom AA. Corrosion inhibition behavior of expired diclofenac Sodium drug for Al 6061 alloy in aqueous media: Electrochemical, morphological, and theoretical investigations. Journal of Molecular Liquids. 2021;343:117656.
7. Niazi H, Yari S, Golestani-Fard F, Shahmiri M, Wang W, Alfantazi A, et al. How deposition parameters affect corrosion behavior of TiO2-Al2O3 nanocomposite coatings. Applied Surface Science. 2015;353:1242-52.
8. Al-Mashhadani HA, Alshujery MK, Khazaal FA, Salman AM, Kadhim MM, Abbas ZM, et al., editors. Anti-corrosive substance as green inhibitor for carbon steel in saline and acidic media. Journal of Physics: Conference Series; 2021: IOP Publishing.
9. Almashhadani H. Synthesis of a CoO–ZnO nanocomposite and its study as a corrosion protection coating for stainless steel in saline solution. Int J Corros Scale Inhib. 2021;10(3):1294-306.
10. Hakimizad A, Raeissi K, Ashrafizadeh F. A comparative study of corrosion performance of sealed anodized layers of conventionally colored and interference-colored aluminium. Surface and Coatings Technology. 2012;206(22):4628-33.
11. Lu X, Mohedano M, Blawert C, Matykina E, Arrabal R, Kainer KU, et al. Plasma electrolytic oxidation coatings with particle additions–A review. Surface and Coatings Technology. 2016;307:1165-82.
12. Ghali E. Corrosion resistance of aluminum and magnesium alloys: understanding, performance, and testing: John Wiley & Sons; 2010.
13. Pornnumpa N, Jariyaboon M. Antibacterial and corrosion resistance properties of anodized AA6061 aluminum alloy. Engineering Journal. 2019;23(4):171-81.
14. Salman T. Kinetic and inhibition effect studies of ecofriendly synthesized silver nanoparticles on lactate dehydrogenase and ferritin activity. Egyptian Journal of Chemistry. 2022;65(3):1-2.
15. AlMashhadani HA. Corrosion protection of pure titanium implant in artificial saliva by electro-polymerization of poly eugenol. Egyptian Journal of Chemistry. 2020;63(8):2803-11.
16. AlMashhadani HA, Saleh KA. Electro-polymerization of poly Eugenol on Ti and Ti alloy dental implant treatment by micro arc oxidation using as Anti-corrosion and Anti-microbial. Res J Pharm Technol. 2020;13(10):4687.
17. AlMashhadani HA, Saleh KA. Electrochemical Deposition of Hydroxyapatite Co-Substituted By Sr/Mg Coating on Ti-6Al-4V ELI Dental Alloy Post-MAO as Anti-Corrosion. Iraqi Journal of Science. 2020:2751-61.